High-content Screen Identifies Cyclosporin A as a Novel ABCA3-specific Molecular Corrector

Maria Forstner[1,3*]; Sean Lin[2,3]; Xiaohua Yang[1]; Susanna Kinting[1]; Ina Rothenaigner[2]; Kenji Schorpp[2]; Yang Li[1]; Kamyar Hadian[2,4,]; Matthias Griese[1,4,]

[1] Department of Pediatric Pneumology, Dr. von Hauner Children's Hospital, Ludwig-Maximilians University, German Centre for Lung Research (DZL), 80337 Munich, Germany.

[2] Assay Development and Screening Platform, Institute of Molecular Toxicology and Pharmacology, Helmholtz Zentrum München, Ingolstaedter Landstr. 1, 85764 Neuherberg, Germany

[3] These authors contributed equally

[4] Equal senior authors

* Funded by Deutsches Zentrum für Lungenforschung, Grant/Award Number: FKZ 82DZL23A2, Friedrich-Baur-Stiftung Reg.-Nr. 51/19

Correspondence: Prof. Dr. Matthias Griese, MD

Dr. von Haunersches Kinderspital, University of Munich, Lindwurmstraße 4,

D-80337 Munich, Germany.

Phone: ++49 89 5160 7870, fax: ++49 89 5160 7872;

e-mail: Matthias.griese@med.uni-muenchen.de

Running title: Cyclosporin A corrects ABCA3-mutants in vitro

Word count for body manuscript: 2570

AUTHOR INFORMATION:

These first authors contributed equally: M.F., S.L.; conceptualization: M.F., S.L., K.H.; M.G.; investigation: M.F., S.L., I.R., K.S., S.K., X.Y., Y.L.; formal analysis: M.F., S.L., I.R.,

AJRCMB Articles in Press. Published December 22, 2021 as 10.1165/rcmb.2021-0223OC

K.S., S.K., X.Y., Y.L.; project administration: M.F., S.L.; writing - original draft: M.F., M.G., K.S., S.L., K.H; writing - review & editing: all authors

This article has an online data supplement, which is accessible from this issue's table of content online at www.atsjournals.org.

AJRCMB Articles in Press. Published December 22, 2021 as 10.1165/rcmb.2021-0223OC

ABSTRACT

ATP-binding cassette (ABC) subfamily A member 3 (ABCA3) is a lipid transporter expressed in alveolar type II cells and localized in the limiting membrane of lamellar bodies. It is crucial for pulmonary surfactant storage and homeostasis. Mutations in the ABCA3 gene are the most common genetic cause of respiratory distress syndrome in mature newborns and interstitial lung disease in children. Apart from lung transplantation, there is no cure available.

To address the lack of causal therapeutic options for ABCA3 deficiency, a rapid and reliable approach is needed to investigate variant-specific molecular mechanisms and to identify pharmacological modulators for mono- or combination therapies. To this end, we developed a phenotypic cell-based assay to autonomously identify ABCA3 wild-type-like or mutant-like cells by using machine-learning algorithms aimed at identifying morphological differences in WT and mutant cells. The assay was subsequently used to identify new drug candidates for ABCA3 specific molecular correction by high-content screening of 1,280 food and drug administration-approved small molecules. Cyclosporin A (CsA) was identified as a potent corrector, specific for some, but not all ABCA3 variants. Results were validated by our previously established functional small format assays. Hence, CsA may be selected for orphan drug evaluation in controlled repurposing trials in patients.

Abstract word count: 202

Key words: ABCA3; ATP-binding cassette subfamily A member 3; childhood interstitial lung disease; chILD; neonatal respiratory distress syndrome; high-content screening; machine learning; cyclosporin A

AJRCMB Articles in Press. Published December 22, 2021 as 10.1165/rcmb.2021-0223OC

INTRODUCTION

The ATP-binding cassette transporter A3 (ABCA3) protein is a phospholipid transporter in alveolar type II cells, which is essential for assembly and homeostasis of pulmonary surfactant and for lysosome-related lamellar body (LB) biogenesis, the storage compartment of surfactant (1-3). Localized to the LB limiting membrane, ABCA3 hydrolyzes ATP to transport phosphatidylcholine and phosphatidylglycerol as major surfactant components into the LB (3-5). Biallelic ABCA3 variants (NM_001089.2) are the most common genetic cause of interstitial lung disease (ILD) in children (chILD) (6-9) and may also play a role in adult ILD (10, 11). So far only 10% of more than 200 described pathogenic ABCA3-variants were functionally classified (12-16). Nonsense and frameshift mutations result in a null phenotype with neonatal respiratory distress syndrome and death within the first months of life, whereas missense, in-frame insertions, deletions, or splicing variants may be compatible with survival (8, 9). Such variants either lead to misfolded ABCA3 proteins, abnormal intracellular trafficking, and retention in the endoplasmic reticulum (ER) (trafficking mutations), or to a reduced ATP mediated phospholipid transport (functional mutations) (12, 17-21). The resulting phenotypes are highly variable and difficult to predict (7, 22). Apart from lung transplantation, no causal therapy is available for ABCA3 deficient patients (9, 23).

A probable approach to treat ABCA3-deficient patients might be modeled in analogy to the treatment of cystic fibrosis (CF) patients. CF is caused by a mutant chloride channel, the CF transmembrane conductance regulator, which is another ABC-transporter (*i.e.,* ABCC7). Here, disease causing mutants can be rescued by small molecules, which have revolutionized treatment (24-27). Recently, we and others have proven this concept *in vitro* for correctors and potentiators of trafficking and functional ABCA3 mutations, respectively (16, 28, 29). Yet, a

AJRCMB Articles in Press. Published December 22, 2021 as 10.1165/rcmb.2021-0223OC

rapid and robust approach to investigate ABCA3 variant-specific molecular mechanisms and to identify pharmacological modulators and combinations of compounds is highly needed.

In this study, we developed a phenotypic cell-based assay, which is compatible with high-content screening (HCS). We utilized the known ABCA3 corrector C13, the ABCA3-variant K1388N, a well-described clinically relevant trafficking mutation (13, 15, 28) and machine-learning algorithms with the aim to unravel ABCA3-specific correctors by screening a library of approved drugs. We identified Cyclosporin A (CsA) and validated it as a potential corrector by using previously described functional small format assays. In addition, we showed that CsA was able to correct several other mistrafficked ABCA3 variants by enabling ABCA3 maturation to wild-type (WT) levels.

METHODS

Cell culture / Treatment of cells

A549 cells stably expressing HA-tagged WT or mutant ABCA3 protein (ABCA3-HA) were cultured and stable cell clones were generated as previously described (13, 28).

Immunoblotting, Immunofluorescence staining, confocal microscopy, TopFluor-PC-transport quantitation

Protein isolation, immunoblotting using 15 µg of total protein, TopFluor-labeled phosphatidylcholine (TopF-PC)-transport quantitation and immunofluorescence staining were performed as previously described (14, 28).

AJRCMB Articles in Press. Published December 22, 2021 as 10.1165/rcmb.2021-0223OC

Screening procedure

Plate and liquid handling were performed using a multi-component high-throughput screening platform. Procedure of cell culture, compound treatment of the cells, immunofluorescence staining and imaging protocols are described in the supplemental file.

Automated image analysis

Multiparametric image analysis was performed using Columbus software version 2.8.0 (PerkinElmer). In the following, the analysis steps in Columbus are described (Fig. S5): GFP and Hoechst signal were smoothened using Median filters to reduce noise signals. Nuclei were detected via the Hoechst signal. The GFP channel was used to define the cytoplasm. In a next step, morphology features (area, roundness, width, length, and ratio width/length) and intensity properties of the Hoechst and the GFP channel (mean, standard deviation, coefficient of variance, median, sum, maximum, minimum, quantile fraction) were calculated for each cell region (nuclei, cytoplasm, and whole cell). In addition, we calculated the texture properties for the whole cell for the GFP and Hoechst channel (SER features, Haralick Features, Gabor Features). Moreover, we applied a filter to remove border objects (nuclei that cross image borders). We performed spot detection using the GFP Channel and calculated again the intensity (GFP signal) and morphology properties of the spots. Next, we used the selection tool 'Linear Classifier' (supervised classification task) to train the software to distinguish between A549 cells expressing mutant K1388N ("K1388N-like cells") and WT ABCA3-HA ("WT-like cells") (using all the properties we calculated before). For training, cells expressing K1388N ("K1388N-like cells") and WT ABCA3-HA ("WT-like cells") were manually selected. After training, the software calculates a classifier according to the linear model (X= -Offset + Linear Coefficient 1*Property 1 + Linear Coefficient 2*Property 2 + ...) and identifies the linear combination of the most relevant properties that determines an effective discriminator for

AJRCMB Articles in Press. Published December 22, 2021 as 10.1165/rcmb.2021-0223OC

"WT-like cells" and "K1388N-like cells".

For hit selection, a threshold of higher than 3 standard deviations from the median of the compound-treated population (% of WT-like cells) was set.

Viability assay

For cell viability experiments, the CellTiter-Glo® 2.0 system (Promega) was performed according to the manufacturer's manual. A549 stably expressing WT or K1388N ABCA3-HA were seeded in 384-well plates and treated with compounds in 10 point-titrations (ranging from 500 μM to 0,977 μM).

Details about chemical correctors, the sample library, the texture properties used for supervised machine learning and statistical analysis are described in the supplementary information.

RESULTS

Development of a HCS-compatible cell-based assay for the identification of ABCA3-specific small molecule correctors

For the identification of molecular correctors of ABCA3 trafficking variants, we established a HCS-compatible robust phenotypic cell-based assay by optimizing various parameters, such as cell density and plate coating (Fig. 1A, Fig. S1). WT ABCA3-HA protein co-localized with the lysosomal marker CD63 in LB like vesicular structures, K1388N ABCA3-HA protein led to smaller vesicles accompanied by a diffuse pattern. Machine learning (ML) analysis was used to recognize cells expressing WT ("WT-like" cells) and K1388N ABCA3-HA ("K1388N-like" cells) by evaluating and weighing differences in various morphological features extracted from a training set of labeled immunofluorescence images (Fig. 1B). These relevant morphological features allowed the ML to significantly discriminate

AJRCMB Articles in Press. Published December 22, 2021 as 10.1165/rcmb.2021-0223OC

WT-like from K1388N-like cells (Fig. 1C). To verify our established image analysis routine, we used the compounds C13 and C17 as positive controls (Fig. S1), which have previously been shown to functionally rescue ABCA3 trafficking variants *in vitro* (16, 28). The ML algorithm was able to reliably classify approximately 86 % of C13-incubated cells expressing K1388N ABCA3-HA as WT-like cells (Fig. 1B).

Identification of hit compounds in a library of 1,280 FDA-approved small molecule drugs

Next, we screened a library of FDA-approved small molecule compounds at a fixed concentration of 10 μM (Fig. 1D). The screening assay quality was determined by Z' factor calculation. Compounds were defined as hits, if they increased the percentage of WT-like cells per well of treated K1388N ABCA3-HA mutant by a number greater than three standard deviations over the median value of the compound-treated population. Calculation of the Z' factor and the signal window showed excellent screening performance (Fig. S1D and data not shown). The screening resulted in 12 hit compounds (Fig. S2A), which were further analyzed. For hit validation, the ratio of cleaved-to-uncleaved ABCA3 was analyzed by western blotting. The detection of uncleaved (190 kDa) and cleaved (170 kDa) ABCA3 protein served as semi-quantitative marker for the identification of ABCA3 trafficking variants. ABCA3 proteins are retained in ER and fail to be glycosylated and proteolytically processed in golgi and post-golgi compartments. Consequently, K1388N ABCA3-HA resulted in a markedly decreased 170/190 kDa ratio (28). To verify the hit compounds, we acquired the 12 hits from independent stocks and treated A549 cells expressing K1388N ABCA3-HA with these hit compounds. The protein level of the processed 170 kDA ABCA3 species was increased by four hit compounds confirming their corrector capacity. Clomipramin hydrochloride (CLI), Cyclosporin A (CsA), doxazosin mesylate (DZN) and R-duloxetine hydrochloride (DX) had strong effects on the ratio of cleaved-to-uncleaved ABCA3 (Fig. S2B). Consistent with the decrease in cleaved-to-

AJRCMB Articles in Press. Published December 22, 2021 as 10.1165/rcmb.2021-0223OC

uncleaved ABCA3, treatment of the cells with CLI, CsA, DZN and DX restored the subcellular localization of K1388N ABCA3-HA in immunofluorescence assays, displaying lysosome-related (anti-CD63) vesicle-like structures as seen in cells expressing WT ABCA3-HA, which indicates restored LB morphology (Fig. S2C). In parallel, dose-dependent toxicity of the hit compounds was assessed via a cell viability assay. 10-point-titrations showed high toxicity to the cells for seven of the 12 hit compounds (pyrvinium pamoate, ivermectin, DX, DZN, CLI, epiandosteron, mitoxantrone hydrochloride); those compounds were therefore excluded from further experiments (Fig. S2D). Together, CsA was the most potent corrector with drug-like properties in the initial screening as well as in the follow-up verification and showed no cellular toxicity. Importantly, CsA is broadly used in other indications for children (30-33) and thus was further evaluated.

Validation of CsA as a molecular corrector for ABCA3 trafficking mutants

CsA dose-dependently increased the number of cells that are classified as WT-like in K1388N ABCA3-HA expressing cells with a half maximal effective concentration (EC_{50}) of 2.8 μM. For comparison, the EC_{50} of the established corrector C13 was 26.4 μM (Fig. 2A). On the protein level, increasing doses of CsA led to an elevated level of the processed 170kDa ABCA3-HA species and thereby raised the 170/190 kDa ratio of K1388N ABCA3-HA (Fig. 2B, Fig. S3A). The quantitation of transport of TopF-PC served as a functional assay for ABCA3 activity (14). CsA significantly increased the function of K1388N ABCA3-HA, as demonstrated by similar ratios of TopF-PC filled vesicles in WT and mutant ABCA3-HA cells after treatment (Fig. 2C).

To test broader applicability of CsA, we evaluated its effect on a larger set of trafficking mutants and one functional mutant (Fig. 3A). We applied ML to distinguish A549 cells expressing WT ABCA3-HA from cells either expressing the trafficking mutant K1388N

AJRCMB Articles in Press. Published December 22, 2021 as 10.1165/rcmb.2021-0223OC

ABCA3-HA or the functional mutant N568D ABCA3-HA. We were successful in distinguishing A549 cells expressing ABCA3-variant N568D from the trafficking mutant in their cellular morphology (Fig. S4A, B). Notably, CsA corrected the trafficking mutants K1388N, A1046E, G1421R and V1399M ABCA3-HA to levels of 50% to beyond 90% WT-like cells. However, the trafficking mutant Q215K was not responsive to CsA treatment (Fig 3B, C). CsA treatment of cells expressing the functional mutant N568D ABCA3-HA only showed a marginal increase in the percentage of WT-like cells (Fig. 3B, C). We further confirmed the imaging-based results by analyzing protein expression levels using Western blotting (Fig. 3D, Fig. S3B). Here, only the trafficking mutants K1388N, A1046E, G1421R and V1399M ABCA3-HA demonstrated an effect. In addition, we showed that the functionality of the N568D ABCA3-protein was not increased as shown by similar percentages of TopF-PC-filled ABCA3+ vesicles and similar relative fluorescence intensity/TopF-PC-filled vesicle upon treatment with DMSO or CsA (Fig. 3E).

Potential mode of action of CsA on ABCA3

CsA inhibits calcineurin by forming a complex with cyclophilin A and acts via calcineurin-independent pathways by inhibiting cyclophilins (34-36). To unravel which of the above mentioned inhibitory pathways of CsA is able to correct ABCA3 variants, we exposed A549 cells expressing K1388N ABCA3-HA to the calcineurin inhibitor pimecrolimus (37), or the cyclophilin inhibitor NIM811 (38), each alone or the combination. Mono treatment with pimecrolimus or NIM811 resulted in a partial rescue of the ABCA3 K1883N-HA-induced trafficking phenotype (Fig. 4B) and increase in processed ABCA3-species (Fig. 4C). The combinatorial treatment of pimecrolimus and NIM811 reverted the trafficking ABCA3 mutant variant phenotype to a comparable level seen with the treatment of CsA (Fig. 4B), although less pronounced in WB assays (Fig. 4C). Together, the individual and synergistic effects of

AJRCMB Articles in Press. Published December 22, 2021 as 10.1165/rcmb.2021-0223OC

pimecrolimus and NIM811 suggests that CsA utilizes calcineurin-dependent as well as calcineurin-independent pathways to correct ABCA3.

DISCUSSION

The purpose of this study was to develop a phenotypic high-content screen to identify small molecule correctors for patients suffering from ABCA3 deficiency and to perform a screen of a library of FDA-approved compounds. We identified 12 hit candidates and evaluated them in conventional assays. CsA was the most promising hit and is a well-known drug safely used in children for decades. Yet adverse effects including immunosuppression, impairment of renal function, and increased blood pressure have to be taken in account. Blood level monitoring is routine in clinical usage of CsA (31-33, 39).

Importantly, by using a linear classifier and training data with labeled images, we were not only able to differentiate WT from mutant cells expressing either WT or the mutant K1388N ABCA3 but were also able to significantly demonstrate and confirm the corrective effect of C13 on K1388N cells (16, 28). Thus, the screening approach should allow the identification of molecules with a comparable or even better effect to C13. Our initial screen hit rate was 0.9 %. Retesting of hit compounds from reordered stocks confirmed selected candidates in the conventional experimental set-up. Our phenotypic assay helped discover corrective compounds without the detailed characterization of the mechanism of a mutation. Here, our ML-based analysis strategy utilized various features like textures, intensity, and morphology to classify WT- and mutant-like cells, thus not relying on detailed molecular understanding of the ABCA3 mutation biology. This is particularly beneficial to test novel compounds on a large set of newly discovered mutants. Importantly, we have established an assay/analysis pipeline that will distinguish WT, trafficking, and functional mutations, which is a valuable resource for future small molecule discovery to identify ABCA3

AJRCMB Articles in Press. Published December 22, 2021 as 10.1165/rcmb.2021-0223OC

potentiators/correctors. Production of cell lines stably expressing newly discovered variants for compound testing could efficiently be accomplished with the landing-pad system (16) with aligned degree of ABCA3 expression.

CsA corrected trafficking of K1388N, A1046E, G1421R and V1399M mutants. However, Q215K, another trafficking variant, was not responsive to CsA (Fig. 3). This variant was also not as susceptible to correction by C13, indicating that this variant might have secondary defects that are not affected by CsA or C13. In line with that, CsA did not improve the transport function of ABCA3 in the functional mutant N568D. CsA was shown to correct trafficking mutants of ABCB4 and ABCB1 in several cell models depending on the underlying variant (40-45). In those studies, evidence was obtained, that CsA led to an improved correction of the mutants through its chaperone abilities, which may be a mechanism also involved in ABCA3 correction, although this needs further validation. In this study, we tested the participation of calcineurin and cyclophilin inhibition in ABCA3 specific correction and their contribution is supported by our results using Pimecrolimus and NIM811 (37, 38). The synergistic effect of pimecrolimus and NIM811 suggests that CsA uses calcineurin and calcineurin-independent pathways to correct ABCA3. These and additional mechanisms, including repression of transcription of mutant ABCA3 protein via reduced NFAT3 signaling through calcineurin inhibition, as suggested by Dave et al. (46) will be a matter of further investigation.

Limitations of the A549 cell model are that it does not account for the patient-specific genetic or environmental background and that only homozygous mutations can be assessed. Also, the impact of ABCA3 overexpression is not scalable. To allow comparisons between WT and different variants, we carefully aligned ABCA3 expression in all stable lines that we

AJRCMB Articles in Press. Published December 22, 2021 as 10.1165/rcmb.2021-0223OC

generated. These limitations may be overcome with patient-derived induced pluripotent stem cells in future studies (47, 48).

ABCA3-deficiency is a rare clinical condition (8) making conventional clinical studies difficult to conduct. Therefore, the screening of FDA-approved drugs and assessing their clinical value in trials may provide an intermediate step towards urgently needed treatments. Repurposing studies have the potential to bridge the time necessary for the development of new molecules, which still have a high rate of failure and take many years until patients may benefit (49, 50). Hence, Cyclosporin A, identified in this work, may be a candidate treatment option in ABCA3 deficiency depending on the responsiveness of the underlying mutation.

ACKNOWLEDGEMENT

We thank Stefanie Brandner for excellent technical assistance.

AJRCMB Articles in Press. Published December 22, 2021 as 10.1165/rcmb.2021-0223OC

REFERENCES

1. Whitsett JA, Wert SE, Weaver TE. Alveolar surfactant homeostasis and the pathogenesis of pulmonary disease. *Annu Rev Med* 2010;61:105-119.

2. Weaver TE, Na CL, Stahlman M. Biogenesis of lamellar bodies, lysosome-related organelles involved in storage and secretion of pulmonary surfactant. *Semin Cell Dev Biol* 2002;13(4):263-270.

3. Ban N, Matsumura Y, Sakai H, Takanezawa Y, Sasaki M, Arai H, Inagaki N. Abca3 as a lipid transporter in pulmonary surfactant biogenesis. *J Biol Chem* 2007;282(13):9628-9634.

4. Yamano G, Funahashi H, Kawanami O, Zhao LX, Ban N, Uchida Y, Morohoshi T, Ogawa J, Shioda S, Inagaki N. Abca3 is a lamellar body membrane protein in human lung alveolar type ii cells. *FEBS Lett* 2001;508(2):221-225.

5. Mulugeta S, Gray JM, Notarfrancesco KL, Gonzales LW, Koval M, Feinstein SI, Ballard PL, Fisher AB, Shuman H. Identification of lbm180, a lamellar body limiting membrane protein of alveolar type ii cells, as the abc transporter protein abca3. *J Biol Chem* 2002;277(25):22147-22155.

6. Shulenin S, Nogee LM, Annilo T, Wert SE, Whitsett JA, Dean M. Abca3 gene mutations in newborns with fatal surfactant deficiency. *N Engl J Med* 2004;350(13):1296-1303.

7. Doan ML, Guillerman RP, Dishop MK, Nogee LM, Langston C, Mallory GB, Sockrider MM, Fan LL. Clinical, radiological and pathological features of abca3 mutations in children. *Thorax* 2008;63(4):366-373.

AJRCMB Articles in Press. Published December 22, 2021 as 10.1165/rcmb.2021-0223OC

8. Wambach JA, Casey AM, Fishman MP, Wegner DJ, Wert SE, Cole FS, Hamvas A, Nogee LM. Genotype-phenotype correlations for infants and children with abca3 deficiency. *Am J Respir Crit Care Med* 2014;189(12):1538-1543.

9. Kröner C, Wittmann T, Reu S, Teusch V, Klemme M, Rauch D, Hengst M, Kappler M, Cobanoglu N, Sismanlar T, et al. Lung disease caused by abca3 mutations. *Thorax* 2017;72(3):213-220.

10. Manali ED, Legendre M, Nathan N, Kannengiesser C, Coulomb-L'Hermine A, Tsiligiannis T, Tomos P, Griese M, Borie R, Clement A, et al. Bi-allelic missense abca3 mutations in a patient with childhood ild who reached adulthood. *ERJ Open Res* 2019;5(3).

11. Klay D, Platenburg M, van Rijswijk R, Grutters JC, van Moorsel CHM. Abca3 mutations in adult pulmonary fibrosis patients: A case series and review of literature. *Curr Opin Pulm Med* 2020;26(3):293-301.

12. Weichert N, Kaltenborn E, Hector A, Woischnik M, Schams A, Holzinger A, Kern S, Griese M. Some abca3 mutations elevate er stress and initiate apoptosis of lung epithelial cells. *Respir Res* 2011;12(1):4.

13. Wittmann T, Schindlbeck U, Höppner S, Kinting S, Frixel S, Kröner C, Liebisch G, Hegermann J, Aslanidis C, Brasch F, et al. Tools to explore abca3 mutations causing interstitial lung disease. *Pediatr Pulmonol* 2016;51(12):1284-1294.

14. Hoppner S, Kinting S, Torrano AA, Schindlbeck U, Brauchle C, Zarbock R, Wittmann T, Griese M. Quantification of volume and lipid filling of intracellular vesicles carrying the abca3 transporter. *Biochim Biophys Acta Mol Cell Res* 2017;1864(12):2330-2335.

AJRCMB Articles in Press. Published December 22, 2021 as 10.1165/rcmb.2021-0223OC

15. Schindlbeck U, Wittmann T, Hoppner S, Kinting S, Liebisch G, Hegermann J, Griese M. Abca3 missense mutations causing surfactant dysfunction disorders have distinct cellular phenotypes. *Hum Mutat* 2018;39(6):841-850.

16. Wambach JA, Yang P, Wegner DJ, Heins HB, Luke C, Li F, White FV, Cole FS. Functional genomics of abca3 variants. *Am J Respir Cell Mol Biol* 2020;63(4):436-443.

17. Matsumura Y, Ban N, Ueda K, Inagaki N. Characterization and classification of atp-binding cassette transporter abca3 mutants in fatal surfactant deficiency. *J Biol Chem* 2006;281(45):34503-34514.

18. Cheong N, Madesh M, Gonzales LW, Zhao M, Yu K, Ballard PL, Shuman H. Functional and trafficking defects in atp binding cassette a3 mutants associated with respiratory distress syndrome. *J Biol Chem* 2006;281(14):9791-9800.

19. Matsumura Y, Ban N, Inagaki N. Aberrant catalytic cycle and impaired lipid transport into intracellular vesicles in abca3 mutants associated with nonfatal pediatric interstitial lung disease. *Am J Physiol Lung Cell Mol Physiol* 2008;295(4):L698-707.

20. Wambach JA, Yang P, Wegner DJ, Heins HB, Kaliberova LN, Kaliberov SA, Curiel DT, White FV, Hamvas A, Hackett BP, et al. Functional characterization of atp-binding cassette transporter a3 mutations from infants with respiratory distress syndrome. *Am J Respir Cell Mol Biol* 2016;55(5):716-721.

21. Beers MF, Mulugeta S. The biology of the abca3 lipid transporter in lung health and disease. *Cell Tissue Res* 2017;367(3):481-493.

22. Bullard JE, Wert SE, Nogee LM. Abca3 deficiency: Neonatal respiratory failure and interstitial lung disease. *Semin Perinatol* 2006;30(6):327-334.

AJRCMB Articles in Press. Published December 22, 2021 as 10.1165/rcmb.2021-0223OC

23. Eldridge WB, Zhang Q, Faro A, Sweet SC, Eghtesady P, Hamvas A, Cole FS, Wambach JA. Outcomes of lung transplantation for infants and children with genetic disorders of surfactant metabolism. *J Pediatr* 2017;184:157-164 e152.

24. Galietta LV, Jayaraman S, Verkman AS. Cell-based assay for high-throughput quantitative screening of cftr chloride transport agonists. *Am J Physiol Cell Physiol* 2001;281(5):C1734-1742.

25. Pedemonte N, Lukacs GL, Du K, Caci E, Zegarra-Moran O, Galietta LJ, Verkman AS. Small-molecule correctors of defective deltaf508-cftr cellular processing identified by high-throughput screening. *J Clin Invest* 2005;115(9):2564-2571.

26. Solomon GM, Marshall SG, Ramsey BW, Rowe SM. Breakthrough therapies: Cystic fibrosis (cf) potentiators and correctors. *Pediatr Pulmonol* 2015;50 Suppl 40(0 40):S3-s13.

27. Van Goor F, Straley KS, Cao D, González J, Hadida S, Hazlewood A, Joubran J, Knapp T, Makings LR, Miller M, et al. Rescue of deltaf508-cftr trafficking and gating in human cystic fibrosis airway primary cultures by small molecules. *Am J Physiol Lung Cell Mol Physiol* 2006;290(6):L1117-1130.

28. Kinting S, Hoppner S, Schindlbeck U, Forstner ME, Harfst J, Wittmann T, Griese M. Functional rescue of misfolding abca3 mutations by small molecular correctors. *Hum Mol Genet* 2018;27(6):943-953.

29. Kinting S, Li Y, Forstner M, Delhommel F, Sattler M, Griese M. Potentiation of abca3 lipid transport function by ivacaftor and genistein. *J Cell Mol Med* 2019;23(8):5225-5234.

AJRCMB Articles in Press. Published December 22, 2021 as 10.1165/rcmb.2021-0223OC

30. Hoyer PF. Cyclosporin a (neoral) in pediatric organ transplantation. Neoral pediatric study group. *Pediatr Transplant* 1998;2(1):35-39.

31. Saracco P, Quarello P, Iori AP, Zecca M, Longoni D, Svahn J, Varotto S, Del Vecchio GC, Dufour C, Ramenghi U, et al. Cyclosporin a response and dependence in children with acquired aplastic anaemia: A multicentre retrospective study with long-term observation follow-up. *Br J Haematol* 2008;140(2):197-205.

32. Henriques Ldos S, Matos Fde M, Vaisbich MH. Pharmacokinetics of cyclosporin--a microemulsion in children with idiopathic nephrotic syndrome. *Clinics (Sao Paulo)* 2012;67(10):1197-1202.

33. Liu AP, Cheuk DK, Lee AH, Lee PP, Chiang AK, Ha SY, Tsoi WC, Chan GC. Cyclosporin a for persistent or chronic immune thrombocytopenia in children. *Ann Hematol* 2016;95(11):1881-1886.

34. Liu J, Farmer JD, Jr., Lane WS, Friedman J, Weissman I, Schreiber SL. Calcineurin is a common target of cyclophilin-cyclosporin a and fkbp-fk506 complexes. *Cell* 1991;66(4):807-815.

35. Ram BM, Ramakrishna G. Endoplasmic reticulum vacuolation and unfolded protein response leading to paraptosis like cell death in cyclosporine a treated cancer cervix cells is mediated by cyclophilin b inhibition. *Biochim Biophys Acta* 2014;1843(11):2497-2512.

36. Schreiber SL, Crabtree GR. The mechanism of action of cyclosporin a and fk506. *Immunol Today* 1992;13(4):136-142.

AJRCMB Articles in Press. Published December 22, 2021 as 10.1165/rcmb.2021-0223OC

37. Grassberger M, Baumruker T, Enz A, Hiestand P, Hultsch T, Kalthoff F, Schuler W, Schulz M, Werner FJ, Winiski A, et al. A novel anti-inflammatory drug, sdz asm 981, for the treatment of skin diseases: In vitro pharmacology. *Br J Dermatol* 1999;141(2):264-273.

38. Billich A, Hammerschmid F, Peichl P, Wenger R, Zenke G, Quesniaux V, Rosenwirth B. Mode of action of sdz nim 811, a nonimmunosuppressive cyclosporin a analog with activity against human immunodeficiency virus (hiv) type 1: Interference with hiv protein-cyclophilin a interactions. *J Virol* 1995;69(4):2451-2461.

39. Cooney GF, Habucky K, Hoppu K. Cyclosporin pharmacokinetics in paediatric transplant recipients. *Clin Pharmacokinet* 1997;32(6):481-495.

40. Andress EJ, Nicolaou M, Romero MR, Naik S, Dixon PH, Williamson C, Linton KJ. Molecular mechanistic explanation for the spectrum of cholestatic disease caused by the s320f variant of abcb4. *Hepatology* 2014;59(5):1921-1931.

41. Delaunay JL, Durand-Schneider AM, Dossier C, Falguières T, Gautherot J, Davit-Spraul A, Aït-Slimane T, Housset C, Jacquemin E, Maurice M. A functional classification of abcb4 variations causing progressive familial intrahepatic cholestasis type 3. *Hepatology* 2016;63(5):1620-1631.

42. Gautherot J, Durand-Schneider AM, Delautier D, Delaunay JL, Rada A, Gabillet J, Housset C, Maurice M, Aït-Slimane T. Effects of cellular, chemical, and pharmacological chaperones on the rescue of a trafficking-defective mutant of the atp-binding cassette transporter proteins abcb1/abcb4. *J Biol Chem* 2012;287(7):5070-5078.

43. Kapoor K, Bhatnagar J, Chufan EE, Ambudkar SV. Mutations in intracellular loops 1 and 3 lead to misfolding of human p-glycoprotein (abcb1) that can be rescued by

AJRCMB Articles in Press. Published December 22, 2021 as 10.1165/rcmb.2021-0223OC

cyclosporine a, which reduces its association with chaperone hsp70. *J Biol Chem* 2013;288(45):32622-32636.

44. Loo TW, Clarke DM. Correction of defective protein kinesis of human p-glycoprotein mutants by substrates and modulators. *J Biol Chem* 1997;272(2):709-712.

45. Park HJ, Kim TH, Kim SW, Noh SH, Cho KJ, Choi C, Kwon EY, Choi YJ, Gee HY, Choi JH. Functional characterization of abcb4 mutations found in progressive familial intrahepatic cholestasis type 3. *Sci Rep* 2016;6:26872.

46. Davé V, Childs T, Xu Y, Ikegami M, Besnard V, Maeda Y, Wert SE, Neilson JR, Crabtree GR, Whitsett JA. Calcineurin/nfat signaling is required for perinatal lung maturation and function. *J Clin Invest* 2006;116(10):2597-2609.

47. Merkert S, Schubert M, Olmer R, Engels L, Radetzki S, Veltman M, Scholte BJ, Zöllner J, Pedemonte N, Galietta LJV, et al. High-throughput screening for modulators of cftr activity based on genetically engineered cystic fibrosis disease-specific ipscs. *Stem Cell Reports* 2019;12(6):1389-1403.

48. Jacob A, Morley M, Hawkins F, McCauley KB, Jean JC, Heins H, Na CL, Weaver TE, Vedaie M, Hurley K, et al. Differentiation of human pluripotent stem cells into functional lung alveolar epithelial cells. *Cell Stem Cell* 2017;21(4):472-488.e410.

49. Pushpakom S, Iorio F, Eyers PA, Escott KJ, Hopper S, Wells A, Doig A, Guilliams T, Latimer J, McNamee C, et al. Drug repurposing: Progress, challenges and recommendations. *Nat Rev Drug Discov* 2019;18(1):41-58.

50. Hoolachan JM, Sutton ER, Bowerman M. Teaching an old drug new tricks: Repositioning strategies for spinal muscular atrophy. *Future Neurology* 2019;14(3):FNL25.

AJRCMB Articles in Press. Published December 22, 2021 as 10.1165/rcmb.2021-0223OC

LEGENDS TO THE FIGURES

Figure 1: High-content screening (HCS) for FDA-approved small molecule ABCA3 correctors

(A) Workflow of the HCS compatible cell-based phenotypic assay: The cells were seeded onto 384-well-plates. After 24 h, compounds were transferred and incubated for another 24 h. The cells were then stained, fixed, analyzed by automated image analysis. Hits were analyzed by employing morphological feature extraction coupled with a machine learning (ML) algorithm to determine "WT-like" and "K1388N-like cells".

(B) Validation of the multiparametric image analysis which distinguishes between "WT-like" cells and "K1388N-like" cells using a ML algorithm. Results were confirmed using 10 μM C13, a previously described ABCA3 corrector. A549 cells stably expressing WT or mutant K1388N ABCA3-HA were treated with 10 μM C13 for 24h and stained for ABCA3-HA. Representative images showing the classified subpopulations by the analysis (cells classified as "WT-like" are marked in green and "K1388N-like" cells in red). Scale bars represent 20 μm. Data are presented as mean (SD) (n=16, mean of a well).

(C) Plot showing the optimized discrimination of "WT-like" versus "K1388N-like" cells by the analysis software after training the system. Circled dots represent the cells used and the color of each indicates the training class. The non-circled dots are the classified objects in the training images and the color indicates the classified class for that object.

(D) Screening of 1,280 FDA-approved compounds on A549 cells expressing K1388N ABCA3-HA. Representative plot of one screening plate is shown. The machine learning (ML) results WT-like cells [%] are sorted by the 24 columns of the screening plate. Hits are highlighted in yellow, including Cyclosporin A (CsA). For hit selection, a threshold larger than 3 standard deviations from the median of the population was set. As negative controls, A549 cells expressing K1388N ABAC3-HA treated with 1% DMSO were used (left and right, orange). As positive controls, A549 cells expressing WT ABCA3-HA (left, green) and A549

AJRCMB Articles in Press. Published December 22, 2021 as 10.1165/rcmb.2021-0223OC

cells expressing K1388N ABCA3-HA treated with 10 µM corrector C13 (right, green) were used.

Figure 2: Validation of CsA as a drug correcting ABCA3 variant K1388N

(A) Dose response curves of cells expressing K1388N ABCA3-HA treated either with CsA or the corrector C13. "WT-like" cells quantified using ML algorithms were plotted in percentage [%]. Concentration of CsA and C13 are shown log10 scale in nM. EC50 are displayed in µM. Data are presented as mean (SD) (n=4).

(B) A549 cells expressing K1388N ABCA3-HA were treated with increasing concentrations of CsA for 24 h and ABCA3-HA protein pattern was analyzed by western blot using anti-HA antibody. Augmentation of the 170 kDa band indicates restored processing of the protein. Results of the densitometric quantitation of protein amount in each band (190kDa and 170kDa) are shown in the supplemental data. UT: untreated.

(C) A549 cells expressing WT or K1388N ABCA3-HA were treated with 10 µM CsA for 24 h, followed by incubation with liposomes containing TopFluor-conjugated phosphatidylcholine (TopF-PC) and treating with 10 µM CsA for another 24 h. The portion of TopF-PC-filled ABCA3+ vesicles was measured. Representative images of the experiment show restored TopF-PC-filled ABCA3+ vesicles of ABCA3-HA variant K1388N upon CsA treatment. Scale bar represents 10µm. Pseudo colors were used consistent with former experiments. Three independent experiments were performed. Results are mean + S.E.M.. ***p<0,001.

Figure 3: CsA corrected other ABCA3-HA variants

(A) Positions of all ABCA3-HA-variants tested in this study were marked in the topology model. Trafficking mutations with abnormal intracellular trafficking of the transporter were marked in red, whereas the functional mutation N568D was marked in blue.

AJRCMB Articles in Press. Published December 22, 2021 as 10.1165/rcmb.2021-0223OC

(B) Representative images of the mutations after 24 h treatment with 10 µM CsA or DMSO control are shown. WT and mutant ABCA3-HA cells were stained against anti-HA. Hoechst was used for nuclear staining. Images were taken using a high-content imaging system. Scale bar represents 10 µm.

(C) Quantitative measurements of ABCA3 trafficking mutants and the functional mutant N568D upon 10 µM CsA or DMSO treatment for 24 h. "WT-like" cells were quantified using ML algorithms are plotted in percentage [%]. Data are presented as mean (SD) (n=16); **p <0,01; ****p<0,0001.

(D) A549 cells expressing A1046E, G1421R, V1399M, Q215K and N568D ABCA3-HA were treated with 10µm CsA for 24 h and ABCA3-HA protein pattern was analyzed by western blot using anti-HA antibody. Augmentation of the 170 kDa band indicates restored processing of the protein. Results of the densitometric quantitation of protein amount in each band (190kDa and 170kDa) are shown in the supplemental data.

(E) A549 cells expressing WT or N568D ABCA3-HA were incubated with liposomes containing TopFluor-conjugated phosphatidylcholine (TopF-PC) and treated with 10 µM CsA for 24 h. Representative images of the experiment show smaller TopF-PC-filled ABCA3+ vesicles of ABCA3-HA variant N568D. The portion of TopF-PC-filled ABCA3+ vesicles and the relative fluorescence intensity/filled vesicle were measured upon treatment with CsA. Scale bar represents 10µm. Pseudo colors were used consistent with former experiments. Four independent experiments were performed. Results are mean + S.E.M..

Figure 4: Treatment with Pimecrolimus and NIM811 restored processing of K1388N ABCA3-HA

(A) A549 cells expressing WT or K1388N ABCA3-HA were treated with 10 µM CsA, 5 µM Pimecrolimus (Pim), 2 µM NIM811 (NIM) and combination of 5 µM Pim and 2 µM NIM

AJRCMB Articles in Press. Published December 22, 2021 as 10.1165/rcmb.2021-0223OC

for 24 h. Representative images of cells stained for ABCA3-HA localization and Hoechst. Scale bar represents 20 µm.

(B) Quantitative analysis of "WT-like cells" of cells expressing either WT or K1388N ABCA-HA by utilizing ML algorithms that allows the recognition. Data are presented as mean (SD) (n=16); ****p<0,0001.

(C) ABCA3-HA protein pattern was analyzed by western blot. Augmentation of the 170 kDa band indicates restored processing of the protein. Densitometric quantitation of protein amount in each band (190kDa and 170kDa) was performed using ImageJ and the ratio of 170/190 kDa was calculated with DMSO treated K1388N set to 1. Results are mean + S.E.M. of four independent experiments. ***p<0,001 in regard to the DMSO vehicle control.

AJRCMB Articles in Press. Published December 22, 2021 as 10.1165/rcmb.2021-0223OC

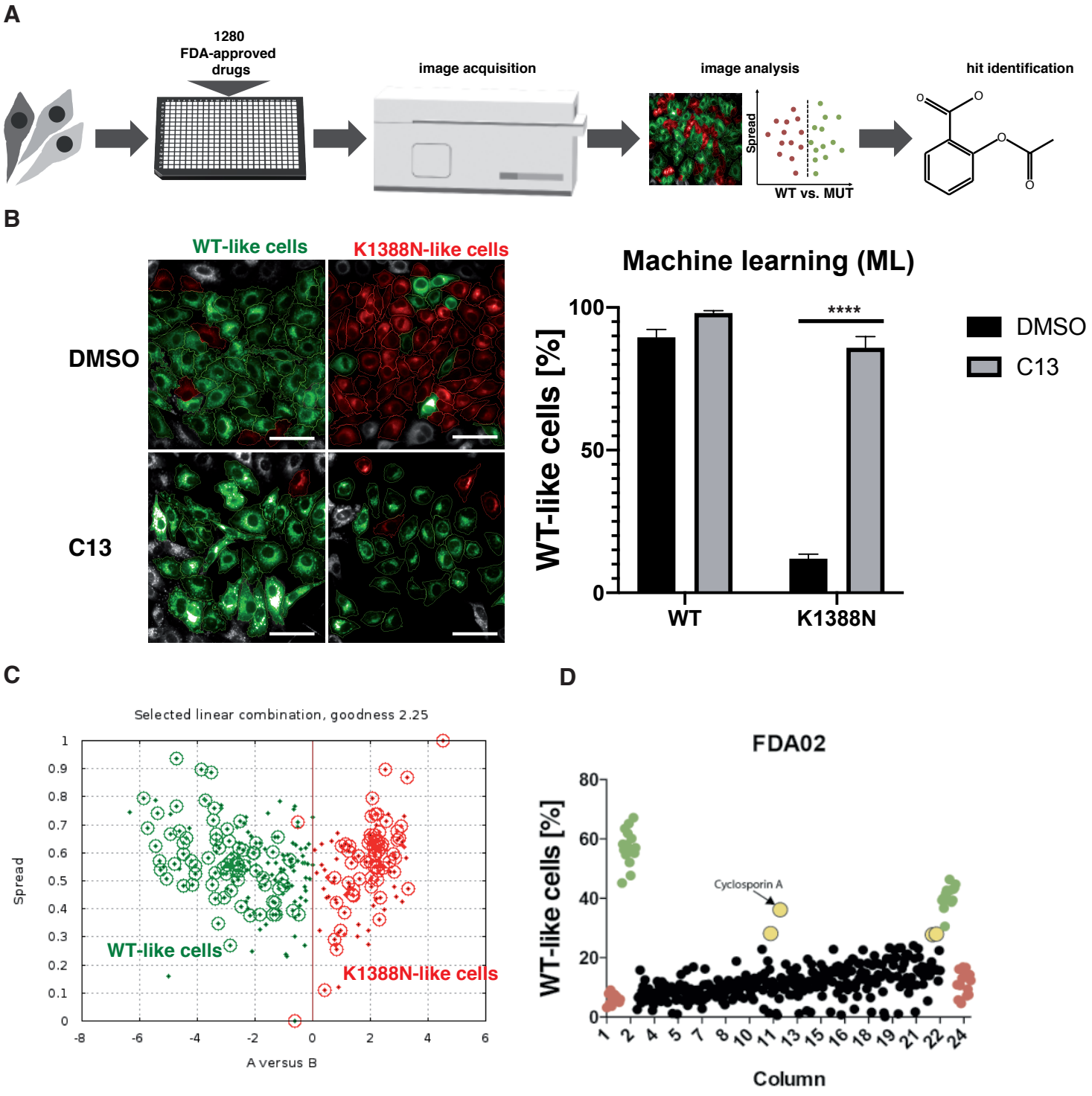

Figure 1

AJRCMB Articles in Press. Published December 22, 2021 as 10.1165/rcmb.2021-0223OC

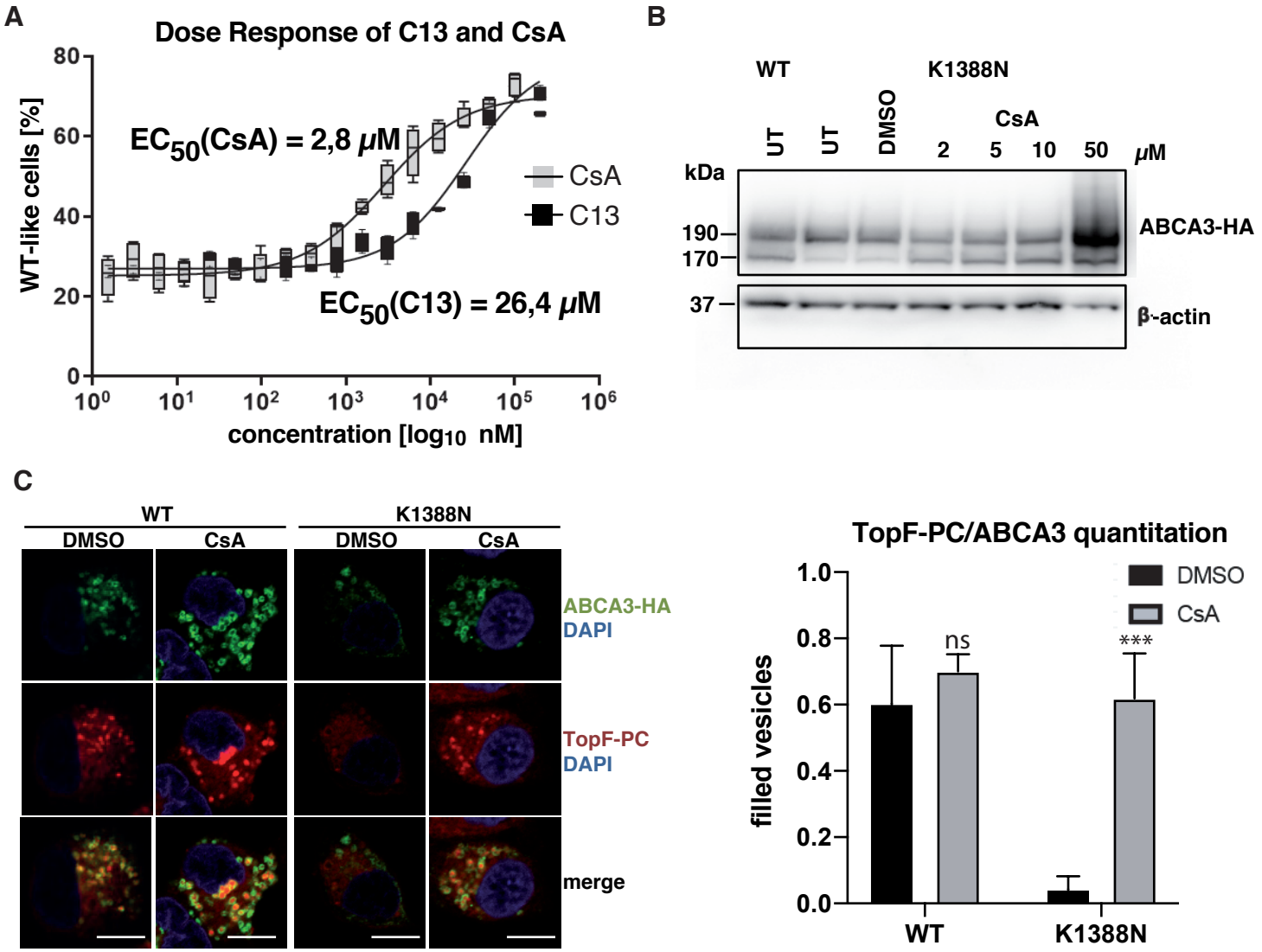

Figure 2

AJRCMB Articles in Press. Published December 22, 2021 as 10.1165/rcmb.2021-0223OC

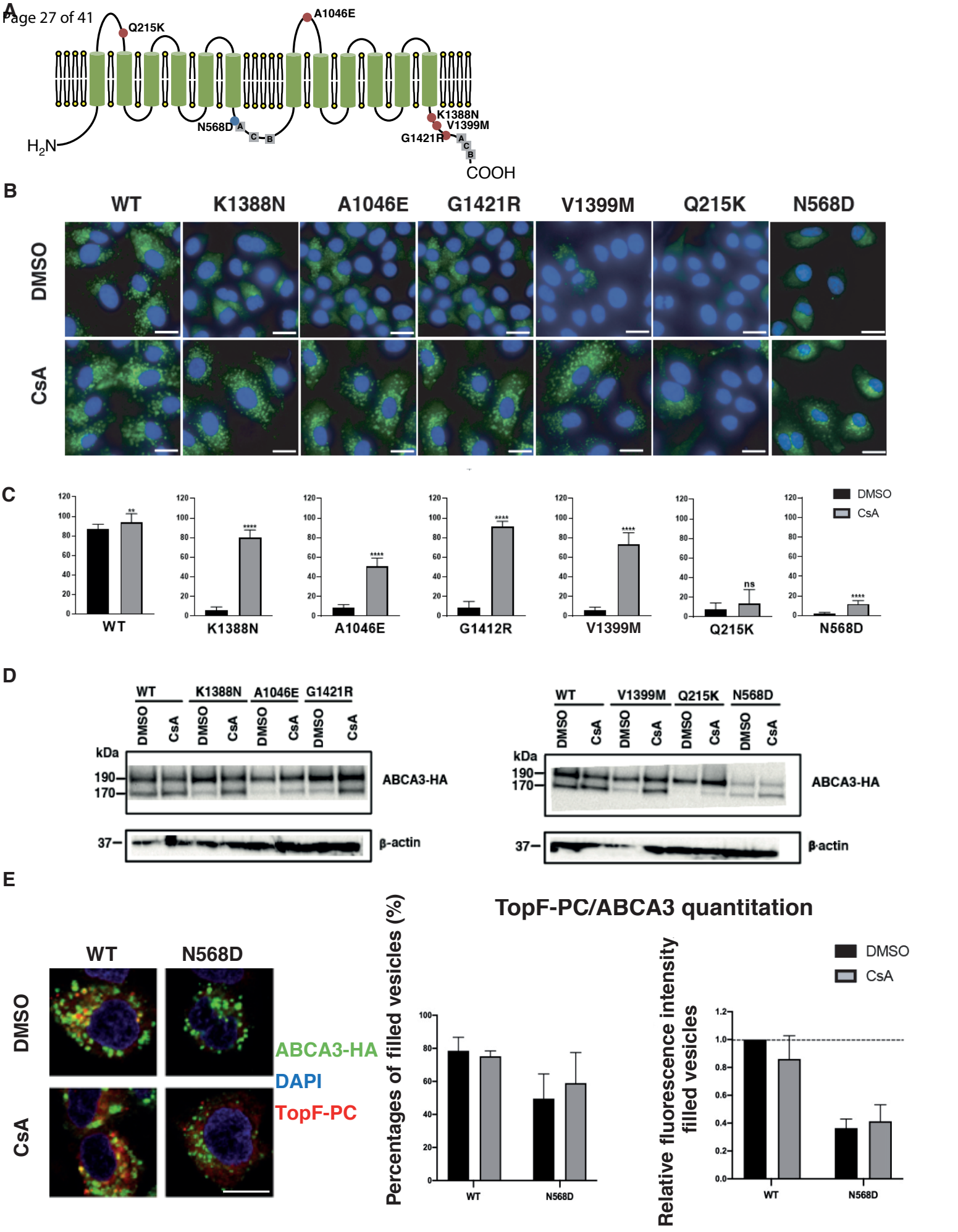

Figure 3

AJRCMB Articles in Press. Published December 22, 2021 as 10.1165/rcmb.2021-0223OC

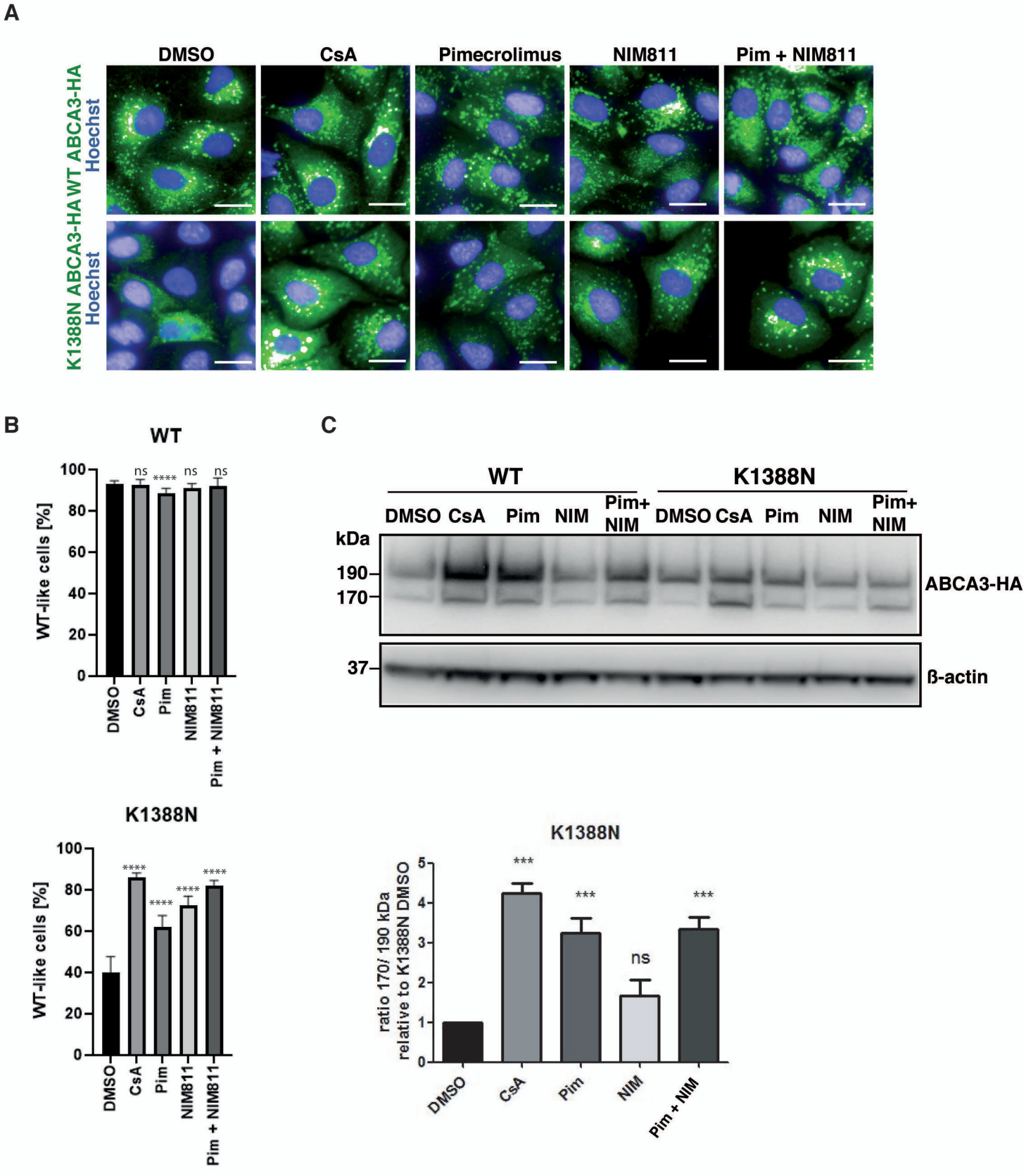

Figure 4

AJRCMB Articles in Press. Published December 22, 2021 as 10.1165/rcmb.2021-0223OC

High-content Screen Identifies Cyclosporin A as a Novel ABCA3-specific Molecular Corrector

Maria Forstner,[1,3*]; Sean Lin,[2,3]; Xiaohua Yang,[1]; Susanna Kinting,[1]; Ina Rothenaigner [2]; Kenji Schorpp,[2]; Yang Li,[1]; Kamyar Hadian,[2,4,]; Matthias Griese,[1,4,]

[1] Department of Pediatric Pneumology, Dr. von Hauner Children's Hospital, Ludwig-Maximilians University, German Centre for Lung Research (DZL), 80337 Munich, Germany.

[2] Assay Development and Screening Platform, Institute of Molecular Toxicology and Pharmacology, Helmholtz Zentrum München, Ingolstaedter Landstr. 1, 85764 Neuherberg, Germany

[3] These authors contributed equally

[4] Equal senior authors

AJRCMB Articles in Press. Published December 22, 2021 as 10.1165/rcmb.2021-0223OC

SUPPLEMENTAL MATERIAL AND METHODS

Chemical correctors / Sample library

Correctors C13 and C17 were obtained from Cystic Fibrosis Foundation Therapeutics (Bethesda, Maryland, USA). The Prestwick Chemical Library (1,280 diverse small molecules, 100% of which are food and drug administration (FDA) approved drugs, Prestwick Chemical Libraries) was preformatted in master plates so that all compounds were solubilized in 100% DMSO at a final concentration of 10 mM. Dinoprost thromethamine salt, Pyrivinium pamoate, Antazoline hydrochloride, Pimecrolimus, NIM811 were obtained from MedChemExpress, Monmouth Junction, New Jersey, Ivermectin, Doxazosin mesylate, Lamotrigin, S-Duloxetin hydrochloride, Tetracylcin hydrochloride, Clomapramin hydrochloride, Mitoxantrone dihydrochloride, Cyclosporin A from Sigma-Aldrich Chemie GmbH, Munich, Germany.

Screening procedure

Plate and liquid handling were performed using a multi-component high-throughput screening platform. 384-well CellCarrier Ultra plates (PerkinElmer) were coated with poly-D-lysine (PDL, Sigma-Aldrich) and excess PDL was washed away. A549 cells stably expressing ABCA3-HA were automatically seeded (7500 cells in 50µl/PDL-coated well) and cultivated for 24 h at 37°C with 5% CO_2. The next day, cells were either treated with 10 µM compound (dissolved in DMSO) or DMSO alone. Final DMSO volume concentration was kept below 1%. Cells were then incubated (37°C, 5% CO_2) for another 24 h prior to fixation with 4% paraformaldehyde (Merck Millipore). Fixed cells were permeabilized with 0.5% TritonX-100 (Sigma). To block non-specific binding sites, cells were incubated in blocking solution (3% Bovine serum albumin (BSA, Sigma) and 10% FBS in PBS). To detect ABCA3-HA protein localization, cells were incubated with anti-HA antibody (Sigma Aldrich) and corresponding AlexaFluor secondary antibody (Life technologies). Nuclei were stained with Hoechst (50

AJRCMB Articles in Press. Published December 22, 2021 as 10.1165/rcmb.2021-0223OC

ng/ml). Cells were imaged on the automated Operetta® High-Content microscope (Perkin Elmer) (40 x high NA objective for high-resolution images). Eight image fields per well were recorded using two channels (Hoechst, GFP). This resulted in an average of 1100 cells that were imaged per well.

Texture properties used for supervised machine learning

The images were analyzed with the high-content analysis software. For this purpose, the nuclei were first identified using the Hoechst signal and, based on this, the cytoplasm and the spots were segmented (Fig. S5). The intensity of the individual channels and the texture and structure of the fluorescence signal were then determined within these cell segments. These features/properties were then used to train the ML model. This enabled to differentiate between different classes (e.g. "WT-like cells" and "K1388N-like cells").

Many of the properties used by the algorithm are texture properties that are calculated for an area of interest. Three methods are available in the Columbus software: SER features, Haralick features and Gabor features. Here is a brief overview of the methods used to calculate texture properties:

Method	Mathematical basis for texture features	Keywords
SER	Gaussian derivative images	Gaussian filter, Gaussian derivative filter, scale-space, edge detection, ridge detection, Laws texture features
Haralick	Co-occurrence matrix	Co-occurrence, Haralick texture features, Robert Haralick
Gabor	Gabor-filtered images	Gabor filter, Gabor texture features, Dennis Gabor

There are eight SER features: Spot, Hole, Edge, Ridge, Valley, Saddle, Bright and Dark. SER is an acronym for Spots, Edges and Ridges. Each SER feature is calculated as intensity of

AJRCMB Articles in Press. Published December 22, 2021 as 10.1165/rcmb.2021-0223OC

a corresponding filtered image averaged over the corresponding object. The four Haralick features calculated are Correlation, Contrast, Homogeneity and Sum Variance. Gabor filter has many parameters. Therefore, this method has more second order parameters than SER and Haralick features. There are two Gabor features calculated at a time: one corresponding to the minimum and the other to the maximum projection of Gabor energy images. Each numerical Gabor feature is intensity of a projection image averaged over the corresponding object. Gabor features have four second order input parameters: Scale, Wavelength, Number of Angles and Normalization.

Statistical analysis

For the conventional assays, two groups were compared with student t-test, multiple groups by one-way analysis of variance with Dunnet's post hoc test. Results were plotted as means ± S.E.M. P-values < 0.05 were considered statistically significant. Tests were performed using GraphPad Prism 7.0 (GraphPad Software, La Jolla, USA).

The quality and robustness of the screening assay was calculated using the Z´ factor as described by Zhang et al.(1) and by calculation of the signal window (SW). Statistical analysis was done using unpaired t-test.

AJRCMB Articles in Press. Published December 22, 2021 as 10.1165/rcmb.2021-0223OC

References

1. Zhang JH, Chung TD, Oldenburg KR. A simple statistical parameter for use in evaluation and validation of high throughput screening assays. *J Biomol Screen* 1999;4(2):67-73.

AJRCMB Articles in Press. Published December 22, 2021 as 10.1165/rcmb.2021-0223OC

LEGENDS TO THE SUPPLEMENTAL FIGURES

Supplemental Figure 1: Development of a high-content screening compatible cell-based assay to identify ABCA3-specific correctors

(A) Images demonstrating the difference between cells expressing WT and K1388N ABCA3-HA upon 1% DMSO, 10 μM C13- and 10 μM C17-treatment after immunofluorescence staining with anti-HA and nuclear staining (Hoechst). Image acquisition was performed by using an Operetta high-content imaging platform.

(B) Cell titration experiments were performed to identify the optimal cell numbers for the 384-well format. 2500, 5000 and 7500 cells/PDL-coated well of cells expressing WT and K1388N ABCA3-HA were seeded and treated as described in (A). Cell image acquisition was performed by using an Operetta high-content imaging platform. Upon seeding 7500 cells/PDL-coated well, cells grew in a confluent monolayer used for the immunofluorescence staining, image acquisition and image-based quantitation.

(C) List of properties (ordered by relevance) and linear coefficients of the linear model used by the Columbus software to distinguish between “WT-like” cells and “K1388N-like “cells.

(D) Calculated Z’ factors for the four screening plates.

Supplemental Figure 2: Hit confirmation and toxicity of the hit compounds

(A) List of 12 compounds, which were identified as hits from the HCS of a library of 1,280 FDA-approved drugs.

(B) A549 cells expressing K1338N ABCA3-HA were exposed to 10 μM hit compounds. Augmentation of the 170 kDa band indicates restored processing of the protein. 10 μm C13 acts as positive control. DMSO: treated with 1% DMSO; UT: untreated; ANT: Antazoline hydrochloride; EpiA: Epiandosteron; DIN: Dinoprost trometamol; Pyr: Pyrvinium pamoate; CsA: Cyclosporin A; TC: Tetracycline; LTG: Lamotrigine; CLI: Clomipramine hydrochloride;

AJRCMB Articles in Press. Published December 22, 2021 as 10.1165/rcmb.2021-0223OC

DZN: Doxazosin mesylate; DHAD: Mitoxantrone hydrochloride; DX: R-Duloxetine hydrochloride; IVM: Ivermectin.

(C) CLI, CsA, DZN, and DX restored subcellular localization of ABCA3-HA variant K1388N. After treatment A549 cells expressing WT or K1388N ABCA3-HA were stained for ABCA3-HA and lysosomal marker CD63. UT: untreated; scale bar expressing 10µm.

(D) Viability assays of the hit compounds from the screening. Cells expressing WT or K1388N ABCA3-HA were treated with the reordered hit compounds and subjected to a cell viability assay. Log 10 concentrations were plotted in [nM], while viable cells were plotted in percentage [%].

Supplemental Figure 3: Densitometric quantitation of ABCA3-HA protein

(A) A549 cells expressing K1388N ABCA3-HA were treated with increasing concentrations of CsA for 24 h and ABCA3-HA protein pattern was analyzed by western blot using anti-HA antibody. Augmentation of the 170 kDa band indicates restored processing of the protein. Densitometric quantitation of protein amount in each band (190kDa and 170kDa) was performed using ImageJ and the ratio of 170/190 kDa was calculated with DMSO treated K1388N set to 1. Results are mean + S.E.M. of three independent experiments. **p<0,01 relating to the DMSO vehicle control.

(B) A549 cells expressing A1046E, G1421R, V1399M, Q215K and N568D ABCA3-HA were treated with 10 µm CsA for 24 h and ABCA3-HA protein pattern was analyzed by western blot using anti-HA antibody. Augmentation of the 170 kDa band indicates restored processing of the protein. Densitometric quantitation of protein amount in each band (190 kDa and 170 kDa) was performed using Image J and the ratio of 170/190 kDa form was calculated with untreated WT set to 1. Results are means + S.E.M. of four (with exception of N568D three) independent experiments. *p<0.05; **p < 0.01; ***p < 0.001 relating to the DMSO vehicle control.

AJRCMB Articles in Press. Published December 22, 2021 as 10.1165/rcmb.2021-0223OC

Supplemental Figure 4: ML-driven classification of WT ABCA3 from trafficking mutant K1388N and functional mutant N568D

(A) A549 cells expressing WT or K1388N or N568D ABCA3-HA were stained for ABCA3-HA. The ML model was trained with images of labeled cells to classify WT, trafficking, and functional variants. Green lined cells indicate that cell was detected from the software as WT-like, red lined cells were identified as trafficking variant-like ("Traff-like"), and blue lined cells as functional variant-like ("Func-like").

(B) Plots showing the optimized discrimination of "WT-like" versus "K1388N-like" cells versus "N568D-like" cells by the trained ML model. Big dots represent the cells used for training of the algorithms. List of properties and linear coefficients of the linear model used by the Columbus Software to classify "WT-like", "Traff-like" and "Func-like" cells.

Supplemental Figure 5: Automated image analysis and machine learning (ML) algorithm.

Illustrative workflow of automated image analysis. For detailed description see material and method section.

AJRCMB Articles in Press. Published December 22, 2021 as 10.1165/rcmb.2021-0223OC

A

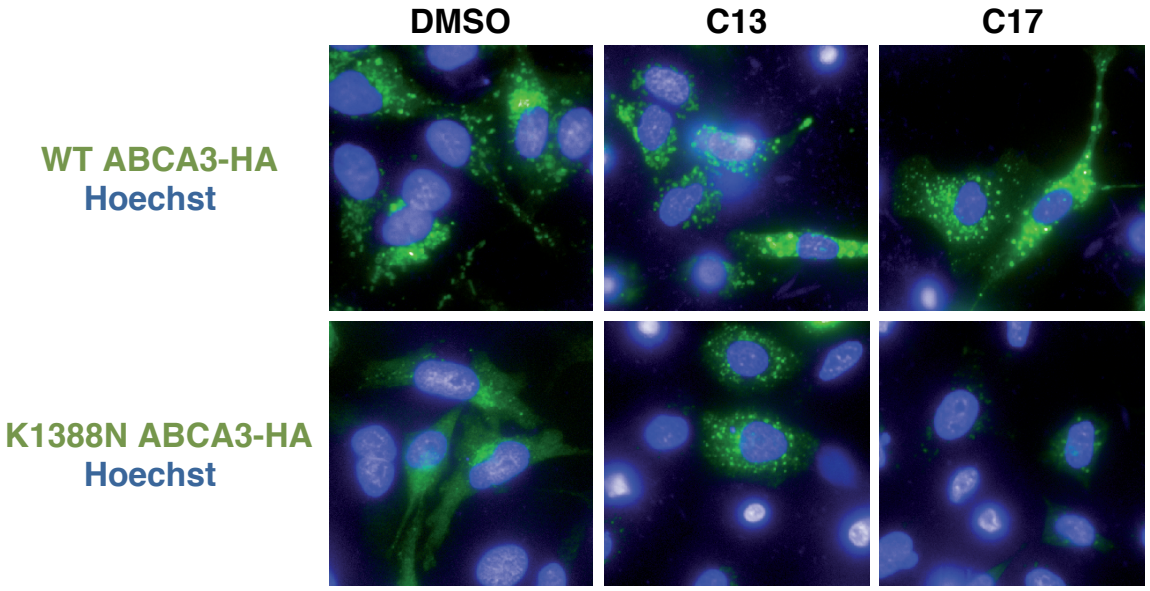

B

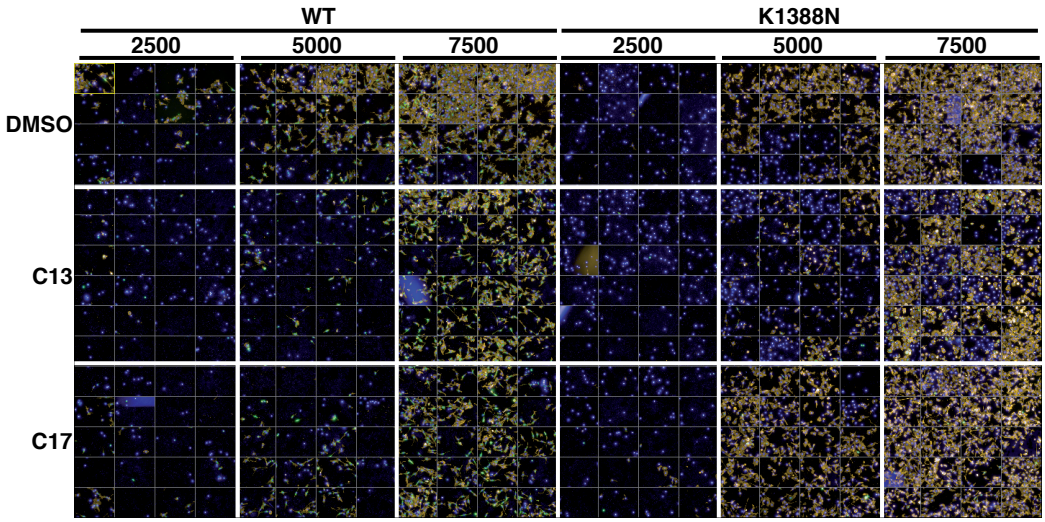

C

Properties (ordered by relevance)	Linear Coefficient
Texture feature SER Spot 1 px (Alexa488)	-4107,72
Texture feature SER Bright 1 px (Alexa488)	925,99
Intensity Cytoplasm Mean (Alexa488)	-0,00063
Texture feature Gabor Min 2 px w2 (Hoechst)	7136,22

D

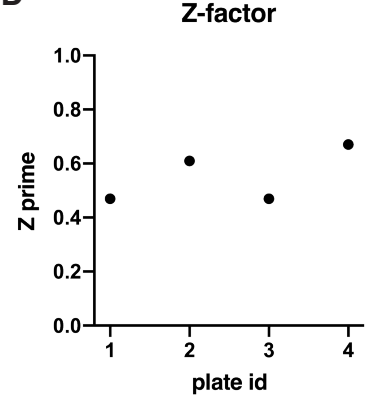

Figure S1

AJRCMB Articles in Press. Published December 22, 2021 as 10.1165/rcmb.2021-0223OC

A

Prestwick ID	Drug	Usage
Prestw-140	Tetracycline hydrochloride	antibiotic
Prestw-258	Antazoline hydrochloride	antihistamine
Prestw-269	Clomipramine hydrochloride	tricyclic antidepressant
Prestw-385	Mitoxantrone dihydrochloride	anti-cancer drug
Prestw-435	Cyclosporin A	immunosuppressive drug
Prestw-440	Epiandrosterone	steroid hormone
Prestw-460	Dinoprost trometamol	abortifacient agents
Prestw-660	Avermectin B1a	anthelmintic drug and pesticide
Prestw-858	Doxazosin mesylate	antihypertensive drug
Prestw-1040	Pyrvinium pamoate	anthelmintic drug
Prestw-1492	Lamotrigine	anticonvulsant medication
Prestw-1708	(R)-Duloxetine hydrochloride	antidepressant

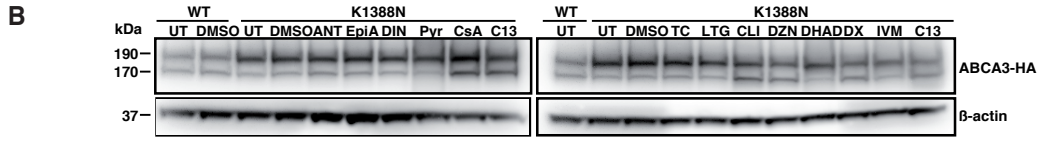

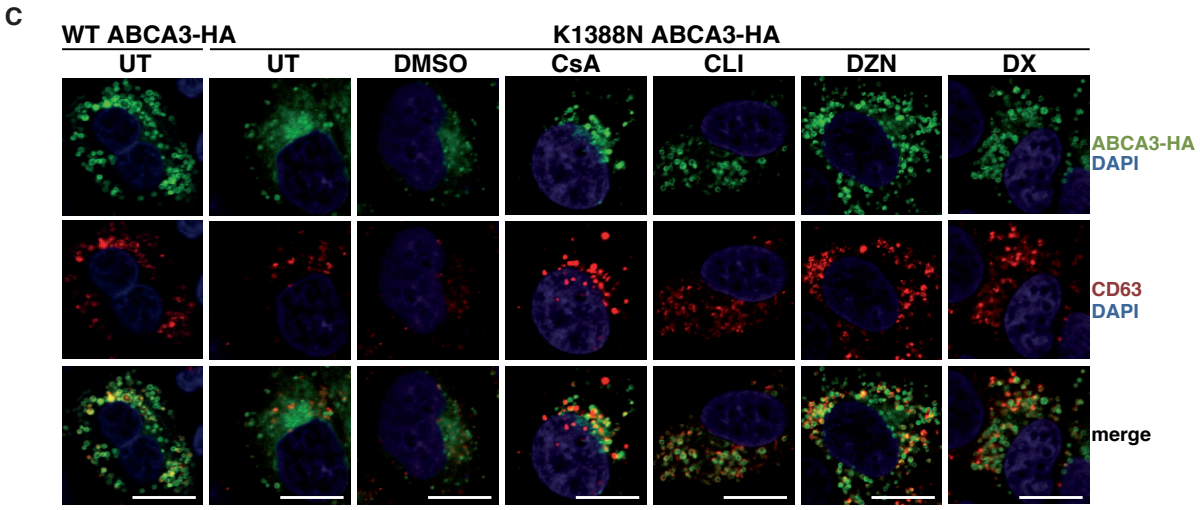

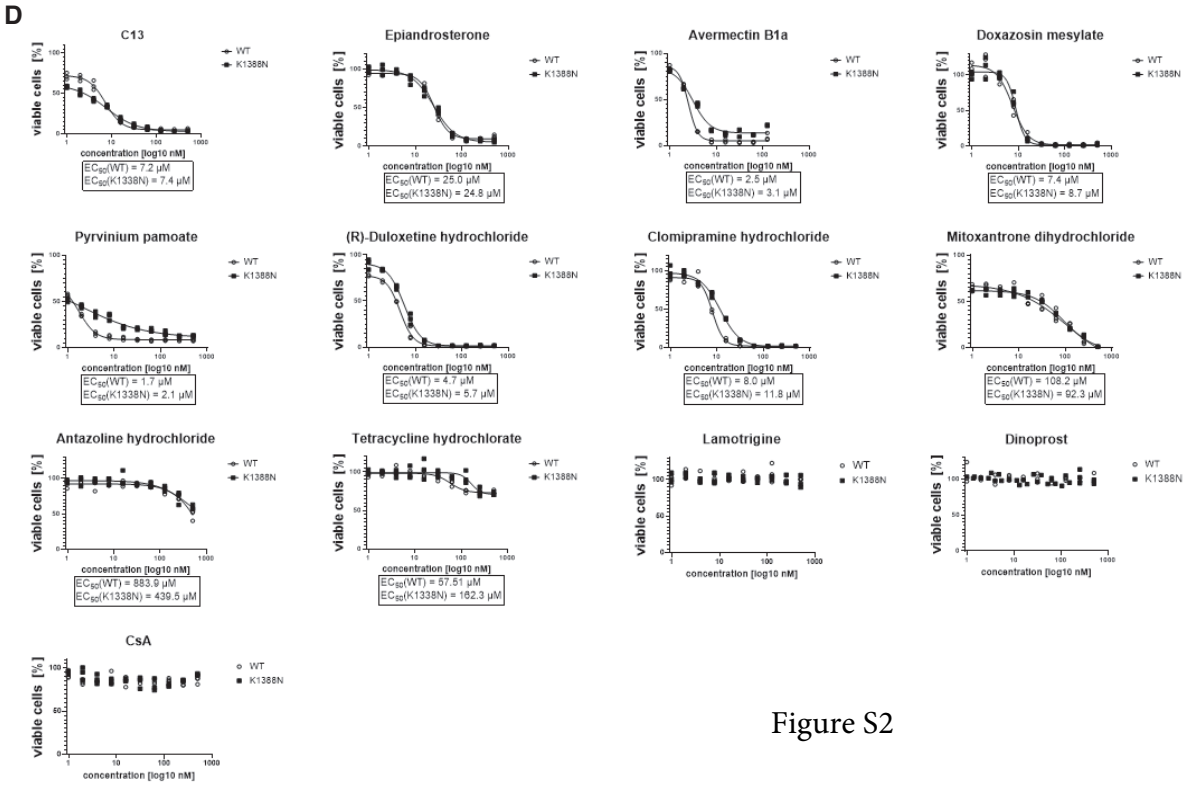

Figure S2

AJRCMB Articles in Press. Published December 22, 2021 as 10.1165/rcmb.2021-0223OC

Figure S3

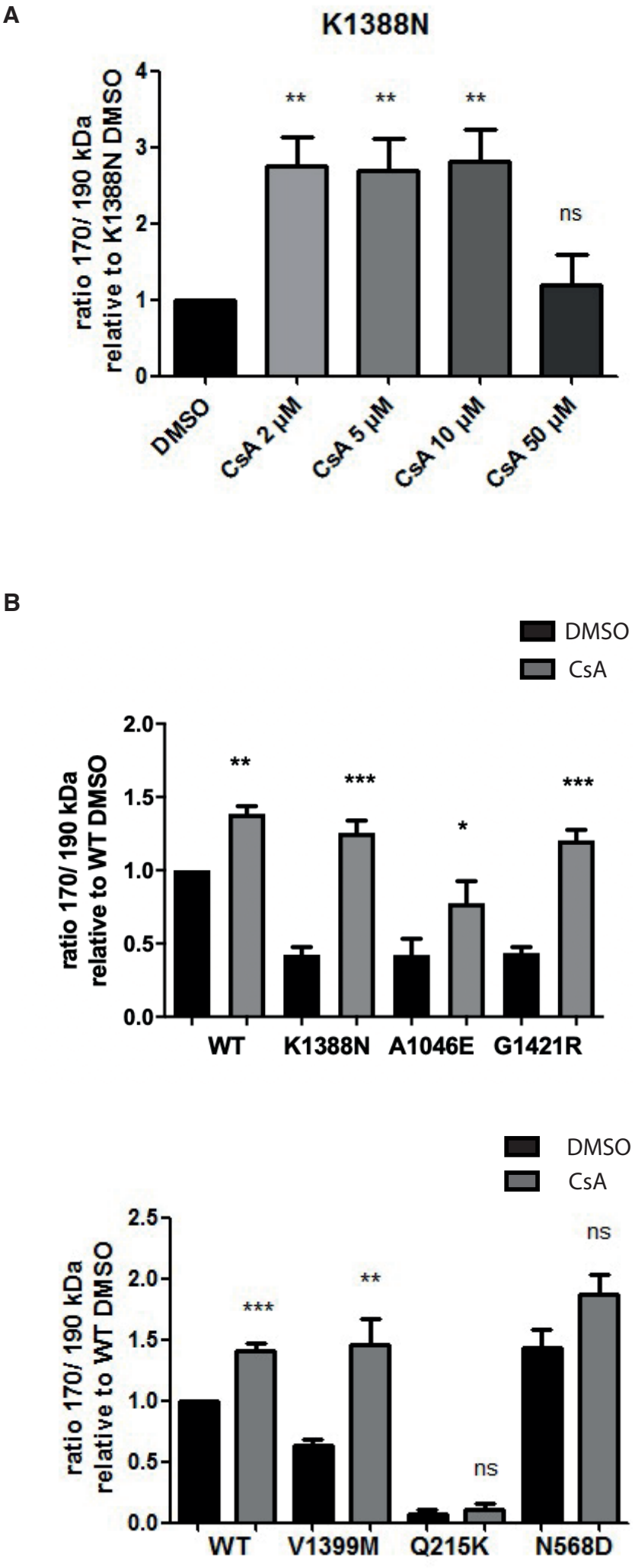

AJRCMB Articles in Press. Published December 22, 2021 as 10.1165/rcmb.2021-0223OC

A

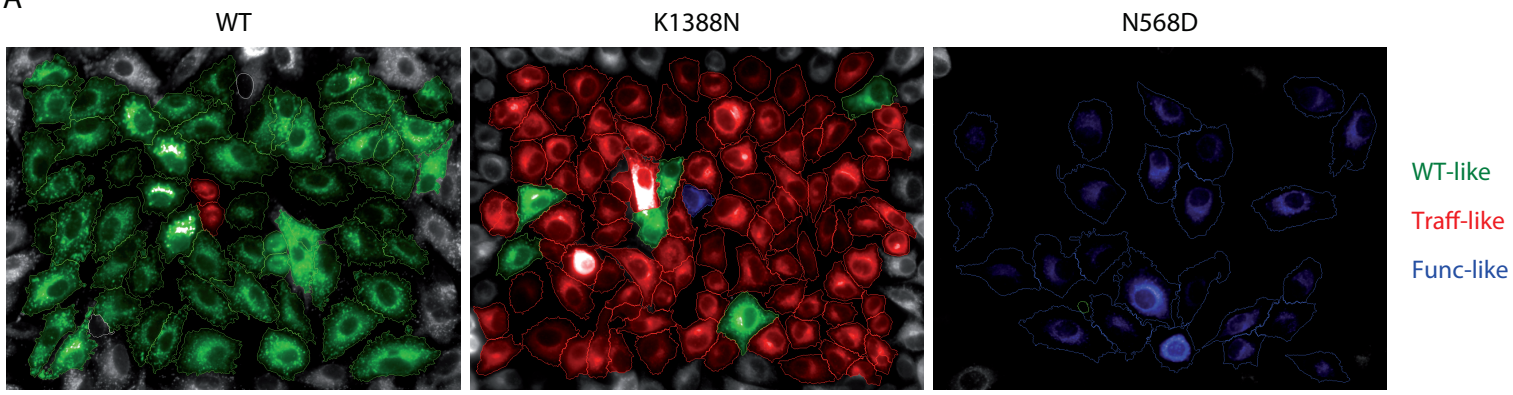

B

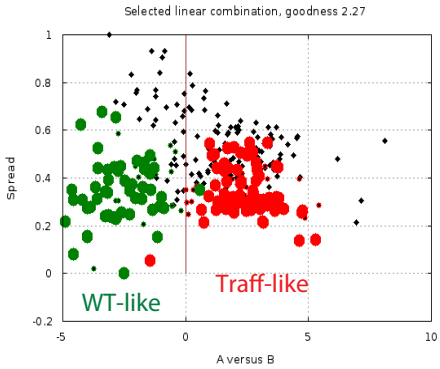

Properties (ordered by relevance)	Linear Coefficient
Texture feature SER Saddle 1 px (Alexa488)	-1017,59
Texture feature SER Edge 1 px (Alexa488)	165,50
Texture feature Haralick Homogeneity 1 px (Alexa488)	33,91
Number of Spots per Area of Cell (Alexa488)	-2285,62
Texture feature Gabor Max 2 px w2 (Alexa488)	4422,32
Texture feature SER Bright 1 px (Alexa488)	627,68
Number of Spots (Alexa488)	0,088
Cytoplasm Length [µm]	-0,058
Texture feature Haralick Sum Variance 1 px (Hoechst)	-1,05
Texture feature Gabor Max 2 px w2 (Hoechst)	-2103,81

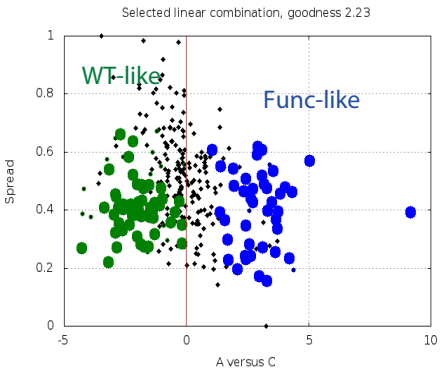

Properties (ordered by relevance)	Linear Coefficient
Texture feature SER Saddle 1 px (Alexa488)	-1011,50
Texture feature SER Saddle 1 px Gabor Max 2 px w2 (Alexa488)	5442,48
Texture feature SER Valley 0 px (Hoechst)	-216,41
Relative Spot Intensity (Alexa488)	42,69

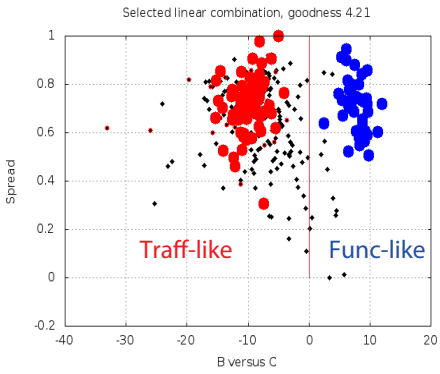

Properties (ordered by relevance)	Linear Coefficient
Texture feature Haralick Correlation 1 px (Alexa488)	325,55
Texture feature SER Valley 1 px (Alexa488)	2594,52
Texture feature Gabor Min 2 px w2 (Alexa488)	95541,86
Texture feature SER Saddle 1 px (Alexa488)	-1423,26
Texture feature SER Edge 1 px (Alexa488)	-293,35
Texture feature Gabor Max 2 px w2 (Hoechst)	-12013,79
Intensity Cytoplasm Mean (Alexa488)	-0.0039
Texture feature SER Ridge 1 px (Alexa488)	-2204,14
Texture feature SER Bright 0 px (Hoechst)	1296,16
Texture feature SER Hole 0 px (Hoechst)	1958,28
Texture feature SER Saddle 0 px (Hoechst)	-1582,11
Cytoplasm Length [µm]	0,13
Texture feature Haralick Sum Variance 1 px (Hoechst)	1,97

Figure S4

AJRCMB Articles in Press. Published December 22, 2021 as 10.1165/rcmb.2021-0223OC

Figure S5

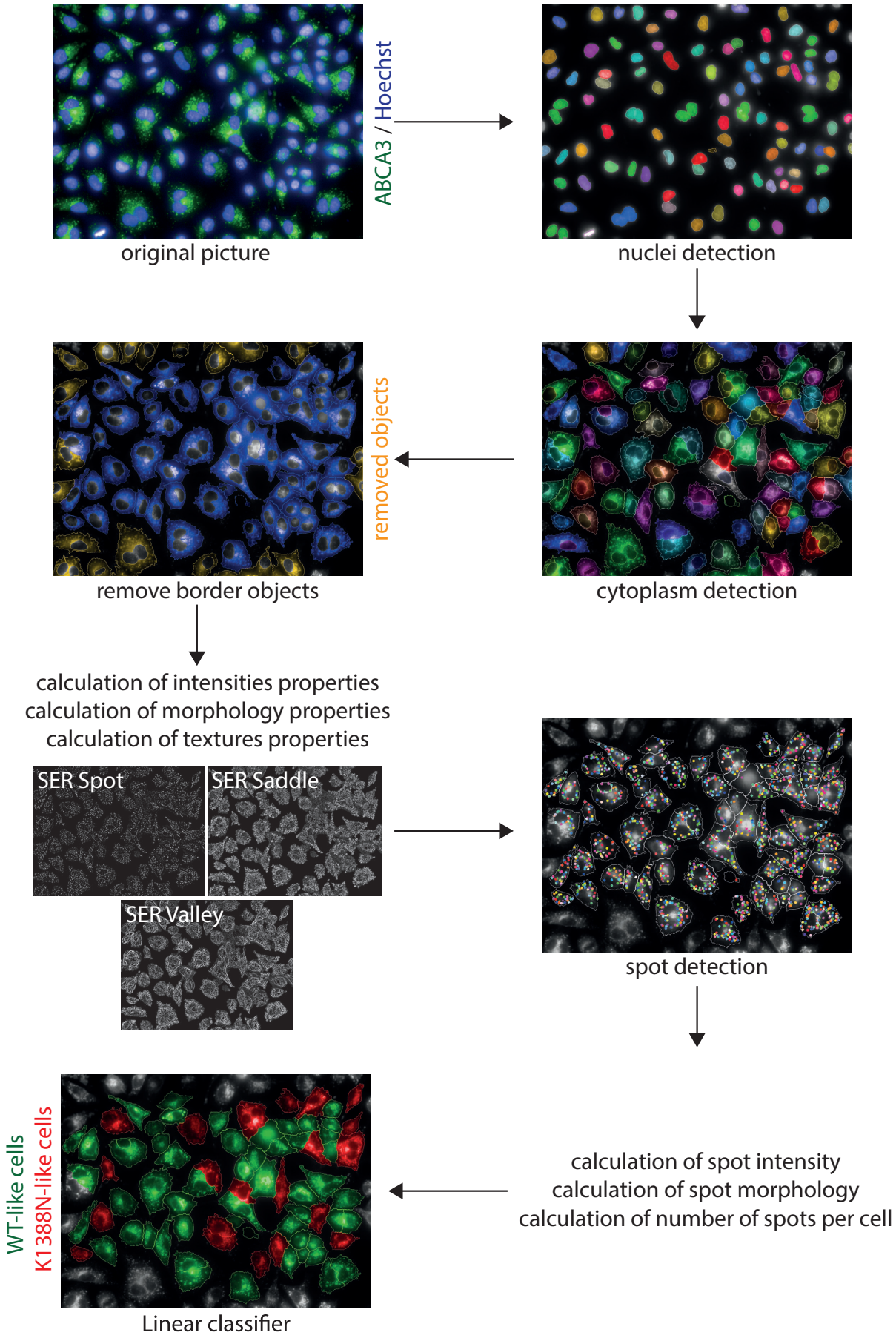

AJRCMB Articles in Press. Published December 22, 2021 as 10.1165/rcmb.2021-0223OC